

MODELING AND TESTING OF A PARABOLIC SOLAR COOKING SYSTEM WITH HEAT STORAGE FOR INDOOR COOKING

N. Mbodji and A. Hajji *

Process Engineering and Environment Research Unit,
Institut Agronomique et Vétérinaire Hassan II
BP 6202-Rabat-Instituts, 10101 Rabat, Morocco
e-mail: ahajji61@hotmail.com, web: <http://www.iav.ac.ma>

Abstract: *This paper presents a dynamic thermodynamic model of a Parabolic Solar Cooking System (PSCS) with heat storage, along with a comparison of the model solution with experimental measurements. The model uses various thermal resistances to take into account heat transfer between the different parts of the system. The first experimental setup consists of a parabolic concentrator (0.80 m diameter and 0.08 m depth) and a 1.57 L cylindrical receiver. The second experimental setup is composed of a parabolic concentrator (1.40 m diameter and 0.16 m depth), the same receiver and a 6.64 L heat storage. Tests were carried out in Rabat, Morocco between April 24th and July 10th, 2014, and between May 15th and June 18th, 2015. Synthetic oil is used as a transfer fluid and a sensible heat storage. Comparison between predicted and measured temperatures shows a good agreement with a relative error of $\pm 4.4\%$.*

Keywords: Modeling, Parabolic Solar Cooking System, Heat Storage, Indoor Cooking

1. INTRODUCTION

With increasing population, economic growth, and environmental concerns, the use of solar energy in domestic cooking is becoming a good alternative for sustainable development which will greatly decrease mortality, deforestation, and soil erosion. The World Health Organization (WHO) reports that each year, 1.6 million people die from respiratory diseases caused by indoor air pollution due to solid fuel use for cooking [1]. A domestic solar cooker saves 100 trees in 15 years of life, prevents annually the release of 1.5 ton of CO₂, increases the household purchasing power (by reducing the budget allocated to cooking), and gives more time to women and children who spend 15 h per week to the chore of wood [1]. While most solar cookers in use today do not have heat storage, this feature will alleviate the mismatch between solar heat energy supply and energy demand for cooking. Heat storage is important for indoor solar cooking requirements and will ensure continuity of service, reduce the use of conventional energy, and give a reasonable cooking time compared with conventional cooking [2]. Modeling solar concentrating systems including parabolic solar cooking systems (PSCS) is a key tool in order to increase their effectiveness and optimize their operating conditions. Several models of solar cookers have been proposed in the last years, but most of them dealt with box and oven types of solar cookers. Very little modeling work considered detailed dynamic temperature distribution and heat transfer in PSCS with storage. Existing models of parabolic solar systems—other than cooking applications—emphasize optimization of power production and not maximizing fluid temperature. In cooking systems, the fluid temperature determines not only the types of food that can be cooked but also the cooking time. There is therefore a need to develop a detailed dynamic model of PSCS with heat storage, which will determine the temperature variations in all system components. The present work is focused on developing such a model and on its experimental validation. The “Methods” section describes the experimental system components and the heat transfer processes involved in its operation. Particular attention was given to the receiver, the key element which absorbs incoming solar radiation, converts it to heat, and transmits it to the heat transfer fluid. The “Results and Discussion” section gives the governing equations derived from heat balance relationships and heat transfer coefficient formulas, describes their numerical solution and presents the model validation by comparison with other known models and with the experimental results obtained from prototype testing.

2. METHODS

2.1. System description and operation

Figure 1 shows the schematics of the experimental system used in this study and described in more details in a previous paper [3]. The system is composed of the following elements: a solar concentrator, a receiver, a heat storage tank, and a circulation pump placed in the primary fluid circuit. Synthetic oil SAE-40 is used as the heat transfer fluid, and the system has a two-axis tracking mechanism.

Figure 2 shows pictures of the second experimental setup. The key part of the PSCS is the receiver also called the absorber which is composed of two black iron cylinders as shown in Figure 3. The inner cylinder, with a volume of 1.57 L, has a thickness of 1.5 mm, a diameter of 0.1 m, and a length of 0.2 m and is black acrylic painted to maximize absorption of solar radiation. The outer cylinder is larger with a thickness of 1 mm, a diameter of 0.2 m, and a length of 0.25 m. The absorber is maintained at the focal point by four square sliding iron tube arms expandable from 0.4 to 0.6 m in length. Glass wool is placed between the two cylinders, as insulation to reduce heat losses. The front of the receiver can optionally be equipped with a glass cover. Table 1 gives the system size parameters

and optical properties of each material in the two devices.

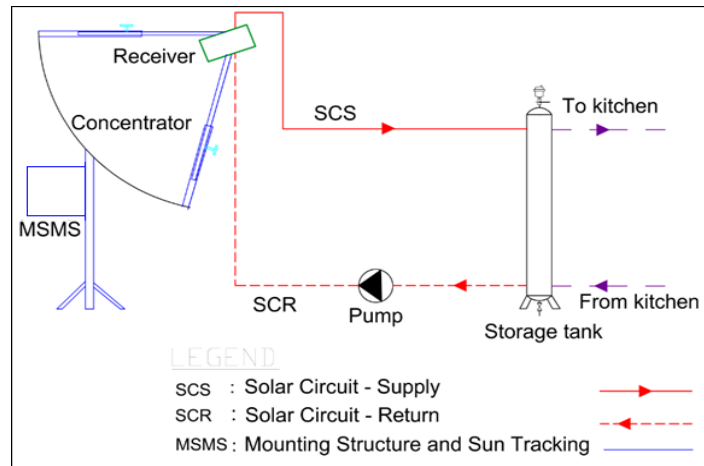


Figure 1. Schematics of a solar cooking system with heat storage

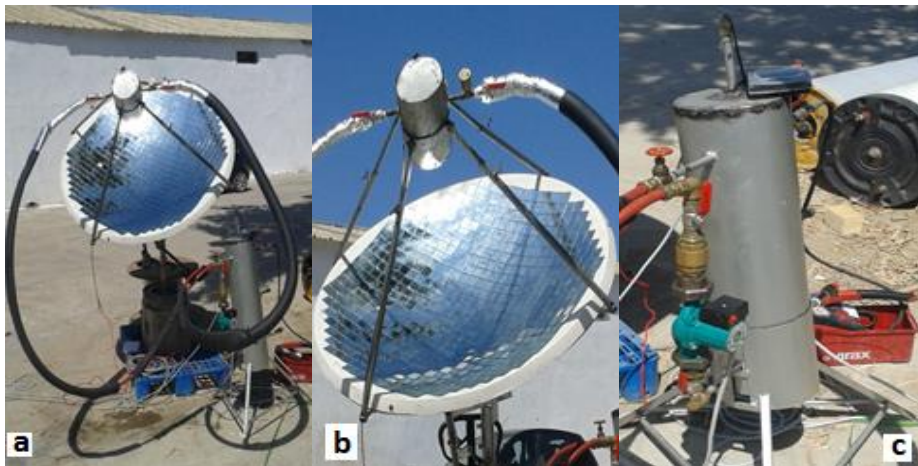


Figure 2. Detailed pictures of the second experimental setup: (a) complete system, (b) concentrator and receiver, (c) heat storage tank and circulation pump

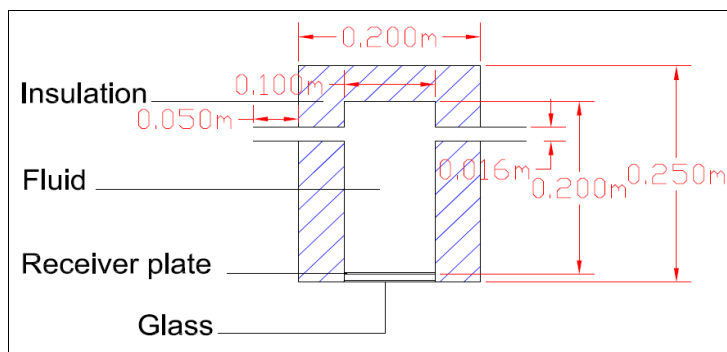


Figure3. Longitudinal section of the receiver

Tableau 1. System size parameters and optical properties

Designation	First experimental device	Second experimental device	Unit
Concentrator			
Diameter	0.8	1.4	m
Depth	0.08	0.16	m
Focal length	0.5	0.77	m
Total mass	5.1	24.7	kg
Surface area	0.353	1.41	m ²
Mirror Reflectance	0.85	*	
Receiver			
Diameter	0.1	*	m
Length perpendicular to the aperture	0.20	*	m
Square sliding tube	0.4-0.6	0.7-0.9	m
Insulation thickness	0.05	*	m
Thickness	1.5	*	mm
Mass	2.34	*	kg
Surface area	0.079	*	m ²
Intercept factor	0.9	*	
Absorptance	0.8	*	
Glass cover			
Diameter	0.12	*	m
Thickness	6	*	mm
Mass	0.23	*	kg
Surface area	0.014	*	m ²
Absorptance	0.01	*	
Transmittance	0.8	*	
Storage			
Diameter		0.12	m
Length		0.65	m
Insulation thickness		0.06	m
Thickness		3.0	mm
Mass		8.97	kg
Surface area		0.26	m ²
*: same value in both systems			

2.2. Heat transfer modes

Incident sunlight reaching the parabolic dish is concentrated on the glass cover at the front face of the receiver. A first part of the concentrated solar radiation is reflected to the ambient, the glass absorbs a second part, and a third part is transmitted through the glass cover. The latter part is absorbed by the receiver plate. A small part is reflected back to the glass cover. Heat is transmitted to the fluid via the black-painted metal absorber. The selective coating layer has a high absorptance and a low emittance in order to reduce thermal radiation losses. Figure 4 shows a cross section of the receiver and all heat transfer processes involved. The absorber is considered to be very rigid, and its properties are not affected by temperature. The thermal resistances and the different modes of heat transfer between the external environment (ambient and sky), the receiver, and the fluid are depicted in Figure 5. We take

into account the energy stored in each node and consider a one-dimensional space temperature variation in the receiver and heat storage tank. The different heat losses, which are conduction through the receiver insulation, convection from the receiver to the ambient air, and radiation from the receiver to the sky, are also considered in a similar manner as Guendouz [4] and Rongrong et al. [5]. For evaluating the different heat loss coefficients, we used the equations presented by Duffie and Beckman [6] and Incropera et al. [7].

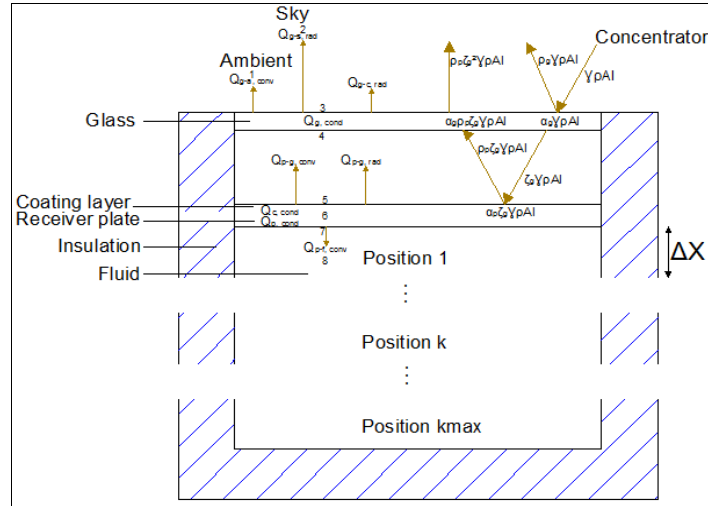


Figure 4. Cross section of the receiver with heat transfer processes

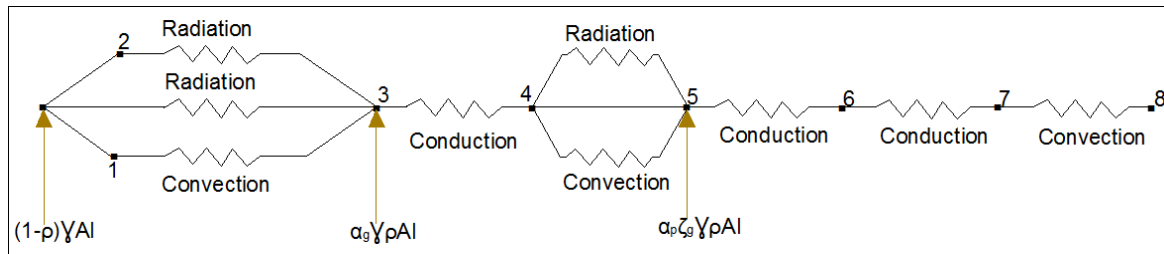


Figure 5. Equivalent thermal resistance model

3. RESULTS AND DISCUSSION

3.1. Governing equations and numerical solution

The present model of the PSCS considers all the above mentioned heat transfer processes, takes into account the presence of the glazing on the receiver, and assumes one-dimensional variations of the temperature along the receiver and the storage tank. The first law of thermodynamics is applied between times t and $t + \Delta t$ to various system components to obtain the governing energy balance equations in a convenient explicit finite difference form ready for numerical solution. For reasons of space, we present only some equations.

For receiver plate, the energy balance is given (from receiver to glass):

$$m_p C_p \Delta T_p = [\alpha_p \tau_g \gamma \rho A_c I_c - h_3 (T_p - T_{f,r}^1) A_p - (h_1 + h_2) (T_p - T_g) A_g] \Delta t \quad (1)$$

At the receiver, the fluid is divided into several zones (from receiver to fluid):

Fluid portion in the position 1 of the receiver:

$$m_{r,k} C_f \Delta T_{f,r}^1 = \left[\dot{m} C_f (T_{f,r}^2 - T_{f,r}^1) + h_3 (T_p - T_{f,r}^1) A_p - \frac{\lambda_f}{\Delta X_r} (T_{f,r}^1 - T_{f,r}^2) A_p - h_g (T_{f,r}^1 - T_a) S_{ur} \right] \Delta t \quad (2)$$

Fluid portion in the intermediate position k ($1 < k < kmax$) of the receiver:

$$m_{r,k} C_f \Delta T_{f,r}^k = \left[\dot{m} C_f (T_{f,r}^{k+1} - T_{f,r}^k) + \frac{\lambda_f}{\Delta X_r} (T_{f,r}^{k-1} - T_{f,r}^k) A_p - \frac{\lambda_f}{\Delta X_r} (T_{f,r}^k - T_{f,r}^{k+1}) A_p - h_g (T_{f,r}^k - T_a) S_{ur} \right] \Delta t \quad (3)$$

Fluid portion in the position $kmax$ of the receiver:

$$m_{r,k} C_f \Delta T_{f,r}^{kmax} = \left[\dot{m} C_f (T_{f,r}^1 - T_{f,r}^{kmax}) + \frac{\lambda_f}{\Delta X_r} (T_{f,r}^{kmax-1} - T_{f,r}^{kmax}) A_p - h_g (T_{f,r}^{kmax} - T_a) (S_{ur} + A_p) \right] \Delta t \quad (4)$$

Similarly, the storage tank is divided into $imax$ fluid zones.

Fluid in the position 1 of the storage tank:

$$m_{s,i} C_f \Delta T_{f,s}^1 = \left[\dot{m} C_f (T_{f,s}^2 - T_{f,s}^1) - \frac{\lambda_f}{\Delta X_s} (T_{f,s}^2 - T_{f,s}^1) A_s - h'_g (T_{f,s}^1 - T_a) (S_{us} + A_s) \right] \Delta t \quad (5)$$

Fluid in the position i ($1 < i < imax$) of the storage tank:

$$m_{s,i} C_f \Delta T_{f,s}^i = \left[\dot{m} C_f (T_{f,s}^{i+1} - T_{f,s}^i) + \frac{\lambda_f}{\Delta X_s} (T_{f,s}^{i+1} - T_{f,s}^i) A_s - \frac{\lambda_f}{\Delta X_s} (T_{f,s}^i - T_{f,s}^{i+1}) A_s - h'_g (T_{f,s}^i - T_a) S_{us} \right] \Delta t \quad (6)$$

Fluid in the position $imax$ of the storage tank:

$$m_{s,i} C_f \Delta T_{f,s}^{imax} = \left[\dot{m} C_f (T_{f,r}^1 - T_{f,s}^{imax}) - \frac{\lambda_f}{\Delta X_s} (T_{f,s}^{imax} - T_{f,s}^{imax-1}) A_s - h'_g (T_{f,s}^{imax} - T_a) (S_{us} + A_s) \right] \Delta t \quad (7)$$

For the resolution, we use the finite difference method. The resolution of the model allows determining the temperature of the concentrator, of the glass, of the plate on the front face of the receiver and the fluid into different zones at the receiver and storage.

The above governing equations are solved numerically to determine the time variations of the temperatures of the concentrator, the glass cover, the plate on the front face of the receiver, and the fluid at different positions both in the receiver and the storage tank.

3.2. Convergence and validation of the numerical solution

The time step is lowered until stability and convergence of the numerical solution is obtained. Figure 6 shows the time variation of the receiver plate temperature at time steps (Δt) 100 s and 10 s, the latter coincide with the curves obtained using smaller values time steps (1s and 0.1s). When the other temperatures are considered, similar behavior is observed, and total stability was obtained with 0.1 s which is the adopted value throughout the present work.

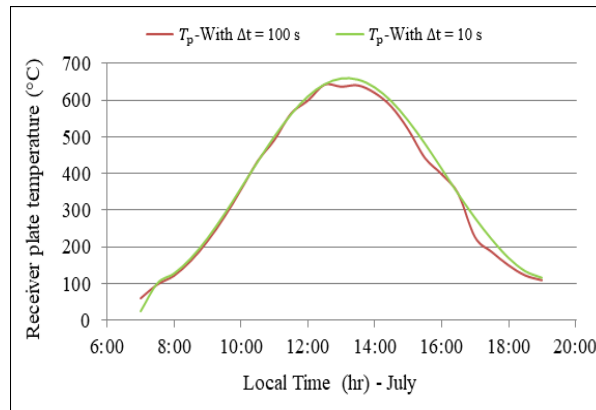


Figure 6. Time variation of the receiver plate temperature at different time steps

Our solution was compared with the results of the simpler model described by Newton [8] which consider that the receiver metal plate and the fluid have the same temperature. Zeghib [9] used the same model but he considers that there is a temperature gradient along the receiver. Figure 7 shows that the temperature difference between the receiver plate and the fluid in position 1 tends to vanish when the heat transfer coefficient is infinite (actually larger than $3,000 \text{ W m}^{-2} \text{ }^\circ\text{C}^{-1}$). Similarly, the temperature difference between the plate and the fluid in position k_{max} decreases to 0 when the fluid thermal conductivity is infinite (actually larger than $2,000 \text{ W m}^{-1} \text{ }^\circ\text{C}^{-1}$).

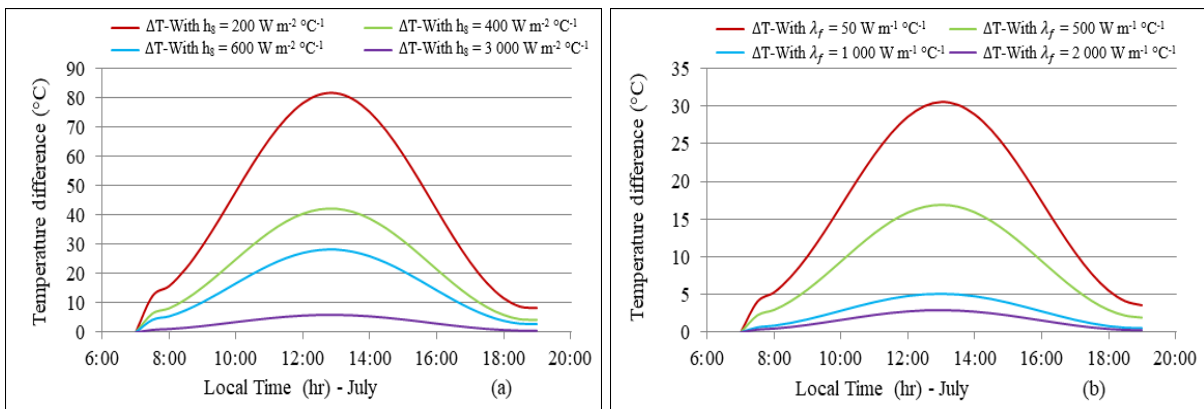


Figure 7. Time variation of the temperature difference between the plate and the fluid when increasing (a) the heat transfer coefficient, and (b) the fluid thermal conductivity

Figure 8 presents the fluid temperature at position k_{max} in the receiver obtained by solving our model using a high heat transfer coefficient (a heat coefficient of $10,500 \text{ W m}^{-2} \text{ }^\circ\text{C}^{-1}$ is taken, to guarantee that the plate temperature and the fluid temperature at position $k = 1$ are equal) and varying the fluid thermal conductivity. At higher values (λ_f) larger than $6,000 \text{ W m}^{-1} \text{ }^\circ\text{C}^{-1}$, the numerical solution matches the one results obtained using the simple model of [8-9], under the same operating conditions and with the same time step (0.1 s).

The first experimental system was tested in the region of Rabat (Morocco) during the period from April 24th to July 10th, 2014. Tests were conducted from 9:00 am to 5:30 pm local time, under clear sky conditions.

Figure 9 compares the measured and the theoretical fluid temperatures in the upper part of the receiver in closed circuit of the first experimental device using SAE-40 synthetic oil at 15-minute intervals which reached a maximum temperature of 153 °C after 5 hours.

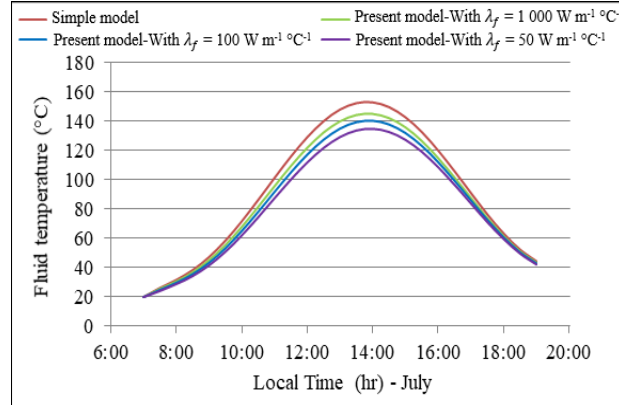


Figure 8. Comparison of the present model with the simple model of [8-9]

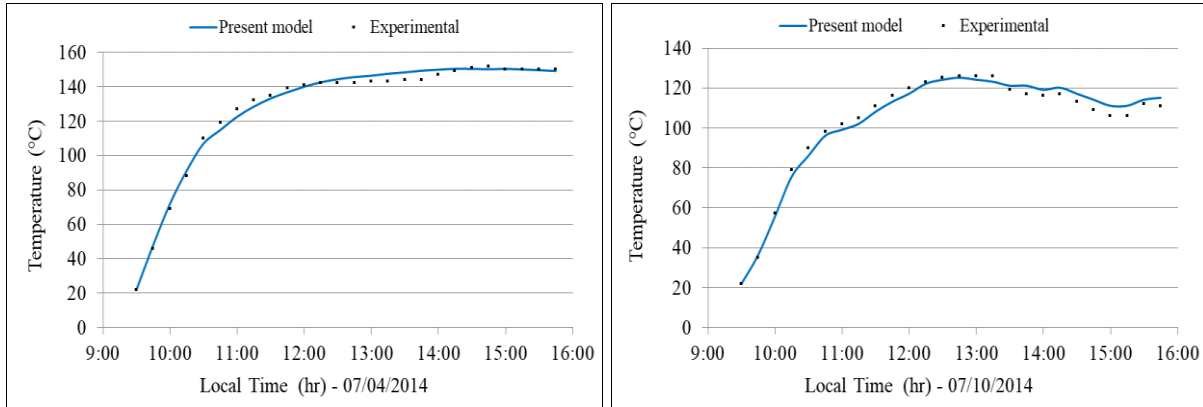


Figure 9. Measured and predicted fluid temperature in the receiver in closed circuit of the first experimental device

The second experimental system was tested at the same location during the period from May 15th to June 18th, 2015 under clear sky conditions.

The measured and the theoretical fluid temperatures in the upper part of the receiver in closed circuit of the second experimental device using SAE-40 synthetic oil at 5-minute intervals are given in Figure 10. The maximum fluid temperature was 150 °C reached after 1 hour of heating.

A good agreement is noticed between the theoretical values and the experimental results. The relative error (RE) is between ± 2.4 and $\pm 4.3\%$, and the root mean square error (RMSE), which represents the arithmetic mean of the squares of the differences between the forecasts and the observations, is between 1.2 and 3.0 °C. These values are summarized in Table 2.

Figure 11 shows the oil temperature measurements in the upper part of the receiver and in the lower part of the storage tank using SAE-40 synthetic oil at 15-minute intervals. The maximum fluid temperature in the storage was 75 °C.

Table 3 summarizes the relative error and the root mean square error which were, respectively,

between ± 4.0 and 5.9% , and between 1.3 and 1.5 °C in the receiver, and between ± 4.4 and $\pm 7.5\%$, and between 1.3 and 1.9 °C in the storage tank. The increase in RE noted on the day of May 27th, 2015 is due to the temperature difference that was greater than 5 °C between the receiver and the storage tank due to the blocking of the pump shaft at the end of the afternoon.

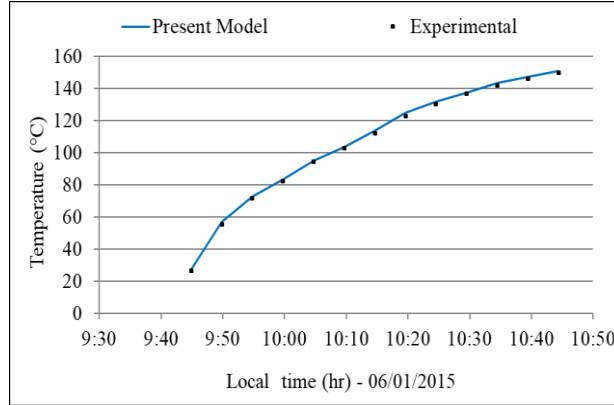


Figure 10. Measured and predicted fluid temperature in the receiver in closed circuit of the second experimental device

Table 2. Relative and root mean square errors in closed circuit

Date	07/04/2014	07/10/2014	06/01/2015
RE (%) - Receiver	± 4.3	± 4.3	± 2.4
RMSE (°C) - Receiver	2.8	3.0	1.2

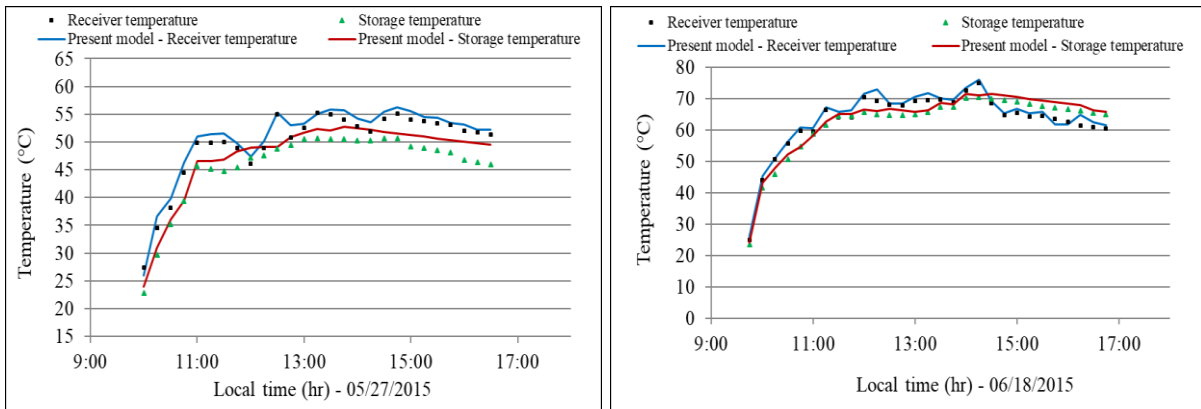


Figure 11. Measured and predicted fluid temperature in the receiver and in the storage tank in open circuit of the second experimental device

Table 3: Relative and root mean square errors in open circuit

Date	05/27/2015	06/18/2015
RE (%) - Receiver	± 5.9	± 4.0
RMSE (°C) - Receiver	1.3	1.5
RE (%) - Storage	± 7.5	± 4.4
RMSE (°C) - Storage	1.9	1.3

4. CONCLUSION

The present model of parabolic solar cooking systems introduced with heat storage for continuous use allowed a valuable analysis of the performance of such systems. Improvement over previous simpler models included a non-uniform receiver temperature and temperature difference between the glass, receiver cover, and thermal fluid. The model-governing equations were solved using an explicit finite difference method, and the method was mathematically validated.

The results of the simulation were compared with experimental results, which proved that the model predicts adequately the thermal behavior of the described system with a relative error $\pm 4.4\%$ and a root mean square error of 3 °C. Therefore, the model is valuable, and can be used to study the operation, to design any of its components, and also to forecast the performance.

The performance of a PSCS can be significantly affected by numerous parameters such as weather conditions (solar radiation, wind) that vary according to the site, material optical properties (reflectance, absorptance, emissivity), system design parameters (aspect ratio, rim angle, intercept factor, exposure ratio), and operating parameters (mass flow rate, glazing, air between the glass and the plate on the front face of the receiver, tracking mechanism, fluid nature, heat losses).

REFERENCES

- [1] ASDER. Solar cookers—Technical presentation. Savoyard Association for the Development of Renewable Energies, Chambéry, France, 2012.
<http://www.asder.asso.fr/phocadownload/cuiseur%20solaire>.
- [2] Prasanna UR. Modeling, optimization and design of a solar thermal energy transport system for hybrid cooking application. PhD thesis, Indian Institute of Science, 2010.
<http://www.utdallas.edu/~prasanna.ur/thesis.pdf>
Mbodji N, Hajji A. Performance testing of a parabolic solar concentrator for solar cooking. *ASME Journal of Solar Energy Engineering*, 2016, 138(4). DOI: 10.1115/1.4033501
- [3] Guendouz B. Use of solar energy for air conditioning needs. Chapter 3: State of the art of solar collectors and modeling. Magister's thesis, Abou Bakr Belkaid University, Tlemcen, Algeria, 2012.
<http://dspace.univ-tlemcen.dz/bitstream/112/1200/1/GUENDOZ-BOUHELAL.pdf>
- [4] Rongrong Z, Yongping Y, Qin Y, Yong Z. Modeling and characteristic analysis of a solar parabolic trough system: thermal oil as the heat transfer fluid. *Journal of Renewable Energy*, 2013. DOI: 10.1155/2013/389514
- [5] Duffie JA, Beckman WA. *Solar engineering of thermal processes*, 2nd edition, New York: John Wiley & Sons, Inc, 1980.
- [6] Incropera F, Dewitt DP, Bergman TL, Lavine AS. *Fundamentals of heat and mass transfer*. 6th edition, New York: John Wiley & Sons, Inc, 2007.
<http://scholarcommons.usf.edu/cgi/viewcontent.cgi?article=4585&context=etd>
- [7] Newton CC. A concentrated solar thermal energy system. Master's thesis, Florida State University, Tallahassee, FL, 2006.
<http://diginole.lib.fsu.edu/islandora/object/fsu:180899/datastream/PDF/view>
- [8] Zeghib I. Design and construction of a parabolic solar concentrator. Master's thesis, Mentouri – Constantine University, Algeria, 2005.

NOMENCLATURE

A_c	concentrator surface area, m ²	T_f	fluid temperature, °C
A_p	receiver plate surface area, m ²	T_g	glass temperature, °C
A_g	glass surface, m ²	T_p	receiver plate temperature, °C
A_s	storage cross section area, m ²	Greek symbols	
C_p	receiver plate specific heat, J kg ⁻¹ °C ⁻¹	α_p	receiver plate absorptance
C_f	fluid specific heat, J kg ⁻¹ °C ⁻¹	γ	intercept factor
h_1	CHTC plate to glass, W m ⁻² °C ⁻¹	Δt	time step, s
h_2	RHTC plate to glass, W m ⁻² °C ⁻¹	ΔX_r	receiver length step, m
h_3	CHTC plaque to fluid, W m ⁻² °C ⁻¹	ΔX_s	storage length step, m
h_p	GHTC receiver to ambient, W m ⁻² °C ⁻¹	λ_f	fluid thermal conductivity, W m ⁻¹ °C ⁻¹
h_g	GHTC storage to ambient, W m ⁻² °C ⁻¹	ρ	mirror reflectance
I_c	direct normal irradiance, W m ⁻²	τ_g	glass transmittance
m_p	receiver plate mass, kg	Sub index	
$m_{r,k}$	receiver fluid partial mass in position k	c	concentrator
$m_{s,i}$	heat storage fluid partial mass in position i	f	fluid
m	thermal fluid mass flow rate, kg s ⁻¹	g	Glass
S_{ur}	receiver lateral surface area, m ²	p	plaque
S_{us}	storage lateral surface area, m ²	r	Receiver
T_a	ambient temperature, °C	s	Storage